MARTIN MARIETTA ENERGY SYSTEMS LIBRARIES
3 4456 0427988 5

CENTRAL RESEARCH LIBRARY
DOCUMENT COLLECTION

OAK RIDGE NATIONAL LABORATORY

operated by

UNION CARBIDE CORPORATION

NUCLEAR DIVISION

for the

U.S. ATOMIC ENERGY COMMISSION

ORNL-TM-3470

cy. 297

DATE - August 1971

ANALYSIS OF BUOYANT JETS WITHIN THE ZONE OF FLOW ESTABLISHMENT

Eric Hirst

OAK RIDGE NATIONAL LABORATORY
CENTRAL RESEARCH LIBRARY
DOCUMENT COLLECTION
LIBRARY LOAN COPY
DO NOT TRANSFER TO ANOTHER PERSON
If you wish someone else to see this document, send in name with document and the library will arrange a loan.

NOTICE This document contains information of a preliminary nature and was prepared primarily for internal use at the Oak Ridge National Laboratory. It is subject to revision or correction and therefore does not represent a final report.

This report was prepared as an account of work sponsored by the United States Government. Neither the United States nor the United States Atomic Energy Commission, nor any of their employees, nor any of their contractors, subcontractors, or their employees, makes any warranty, express or implied, or assumes any legal liability or responsibility for the accuracy, completeness or usefulness of any information, apparatus, product or process disclosed, or represents that its use would not infringe privately owned rights.

CONTENTS

Page

NOMENCLATURE iv

ABSTRACT 1

1. INTRODUCTION 1

2. DEVELOPMENT OF THE INTEGRAL METHOD 6

3. RESULTS OBTAINED WITH THE METHOD 13

4. SUMMARY 17

REFERENCES 19

APPENDIX A: EVALUATION OF THE INTEGRALS IN THE DIFFERENTIAL EQUATIONS 21

APPENDIX B: EVALUATION OF THE DIFFERENTIAL EQUATIONS 24

APPENDIX C: FIGURES 29

MARTIN MARIETTA ENERGY SYSTEMS LIBRARIES

3 4456 0427988 5

Nomenclature

a_i, A_i	dimensionless coefficients in the entrainment equation
a_{ij}, A_{ij}	coefficients in equations (20) and (21)
b	jet width
c	concentration
C_i	$\cos \Theta_i$
$C\phi$	$\cos \phi$
d_i	shorthand notation, defined in Appendix B
E	entrainment rate
f_i, F_i	coefficients in equations (20) and (21)
Fr	Froude number, $u_0^2/\left[(\rho_\infty - \rho_0)\ r_0 g/\rho_0\right]$, dimensionless
g	acceleration of gravity, 32.174 ft/sec^2
$\bar{i}$, $\bar{j}$, $\bar{k}$	unit vectors parallel to the x, y, z axes, respectively
i_s, i_r, i_ϕ	unit vectors parallel to the s, r, ϕ axes, respectively
I_i	integrals, defined in Appendix A
q	$\int_0^\infty \bar{u}^2\ r dr - \frac{1}{4} E^2$
r	radial distance from jet centerline
r_c	width of the concentration potential core
r_t	width of the temperature potential core
r_u	width of the velocity potential core
R	velocity ratio, u_∞/u_0
R_{12}	$R \cdot \sin \Theta_1 \cdot \cos \Theta_2$
s	streamwise coordinate, distance along the jet axis
S_i	$\sin \Theta_1$
$S\phi$	$\sin \phi$

t	temperature
u	component of velocity parallel to $\bar{i}_s$
u_{12}	$u \cdot \sin \theta_1 \cdot \cos \theta_2$
x	cartesian coordinate, horizontal and perpendicular to freestream
y	cartesian coordinate, horizontal and parallel to freestream
z	cartesian coordinate, positive vertically up
ZEF	zone of established flow
ZFE	zone of flow establishment, defined as the region in which the centerline velocity remains constant and equal to u_o
β	thermal coefficient of volumetric expansion, $-\frac{1}{\rho_0}\left(\frac{\partial \rho}{\partial t}\right)_p$
γ	concentration coefficient of volumetric expansion, $-\frac{1}{\rho_0}\left(\frac{\partial \rho}{\partial c}\right)_t$
θ_1	angle between the projection of $\bar{i}_s$ onto the x,y plane and the x axis
θ_2	angle between $\bar{i}_s$ and the x, y plane
λ	spreading ratio between density and velocity profiles
ρ	density
ϕ	azimuthal angle
$(\ )_o$	at diffuser outlet, $s = 0$
$(\ )_m$	at jet centerline, $r = 0$
$(\ )_{th}$	top-hat value
$(\ )_\infty$	freestream value
$(\ )_e$	at end of flow establishment zone
$(\ )'$	derivative with respect to s
$(\bar{\ })$	average with respect to time
$\Delta(\ )$	$(\ ) - (\ )_\infty$

ANALYSIS OF BUOYANT JETS WITHIN THE ZONE OF FLOW ESTABLISHMENT

Eric Hirst

Abstract

In order to assess the ecological consequences of thermal discharges from steam-electric power plants, one must be able to predict the physical changes (temperature, velocity, salinity) induced by these discharges. This work is concerned with the mathematical prediction of these physical properties in the zone of flow establishment (ZFE), for thermal effluents discharged as buoyant jets through round, submerged diffusers. The ZFE is the region, immediately beyond the diffuser exit, in which the mean flow profiles undergo a transition from their internal flow shapes to a free turbulent flow condition.

The method developed here uses the integral equations of mass, energy, salt, and momentum conservation. The solution to these equations includes the length of the ZFE, and the values of jet width, jet orientation, and centerline temperature and salinity at the end of this zone. This method is quite general, capable of predicting buoyant jets with three dimensional trajectories discharged to flowing, stratified ambients.

Results obtained with the method agree well with the limited experimental data available and with existing semi-empirical correlations. Unfortunately, the range of flow variables covered by the data and correlations is quite small. Predictions of starting length, jet width, centerline temperature, and jet orientation at the end of the ZFE are presented for several Froude number:velocity ratio:initial orientation combinations.

This method can be used to provide the necessary initial conditions for conventional (applicable only in the zone of established flow) buoyant jet prediction methods. Further, the method can be used to help design optimal thermal discharge configurations.

1. Introduction

Modern steam-electric power plants discharge approximately 1.5–2 kwh of waste heat for every kwh of electrical energy produced. Traditionally, this heat has been discharged to a water body adjacent to the power plant using "once-through" cooling. With this method, water is pumped through

the condensers, where its temperature is increased 10°–30°F, and then discharged back into the receiving water body. Because aquatic organisms tend to be temperature sensitive, these massive thermal discharges modify the local aquatic environment.

Biological models exist which describe the response of aquatic organisms to their time-temperature history. This time-temperature history is defined by engineering models which predict the physical changes (temperature, velocity salinity) induced by thermal discharges. These models must be integrated to yield predictions of the ecological effects of power plant thermal discharges. This work is concerned with the prediction of physical properties for thermal effluents discharged as buoyant jets through single, circular, submerged diffusers. Attention is restricted to the region immediately beyond the diffuser exit, the zone of flow establishment (ZFE).

The method developed here uses the integral equations of mass, energy, salt, and momentum conservation. The solution includes the length of the ZFE, and the values of jet width, jet orientation, and centerline temperature and salinity at the end of this zone. This method is quite general, capable of predicting buoyant jets with three dimensional trajectories discharged to a flowing, stratified ambient.

To the author's knowledge this is the first such method described in the literature. Several semi-empirical correlations exist but they are limited in applicability.

In general, round buoyant jets pass through several regimes as they move from the diffuser outfall through the ambient. The three most commonly considered regimes are (see figure 1):

a. Zone of flow establishment (ZFE) - in which the mean flow profiles undergo a transition from their internal flow shapes to a free turbulent flow condition. It is in this region that mixing begins with the ambient fluid. Here the flow is strongly influenced by the outfall conditions and only slightly influenced by ambient conditions. Within the ZFE the centerline velocity remains constant, equal to u_o.

b. Zone of established flow (ZEF) - begins when turbulent mixing has reached the jet centerline, and the centerline velocity begins to decay. In this region the profiles have assumed their free turbulent shapes and

the jet dynamics are governed by the jet's momentum and buoyancy and the free stream conditions, rather than by the initial outfall conditions.

c. Field zone - in which the jet momentum is depleted and the jet fluid is convected and diffused by the ambient currents and ambient turbulence.

The zone of established flow has been extensively studied, both experimentally and theoretically,[1-3] but the other two regions have received much less attention.

Some experimental data concerning the length and shape of the ZFE is available. Albertson, et al.[4] showed that the length of this region, s_e, is:

$$s_e/r_o = 12.4 \tag{1}$$

and that the shape of the potential core is roughly conical, with

$$r_u/r_o = 1 - s/s_e \tag{2}$$

for a simple momentum jet, i.e., a non-buoyant jet discharged to a quiescent ambient. The width of the free-turbulent region grows linearly as:

$$b/s = 0.115 \tag{3}$$

so that $b_e/r_o = \sqrt{2}$ for a simple momentum jet. Figure 2 is a sketch of the ZFE (for a more general flow) showing the potential core and the free-turbulent flow.

The velocity profile within the ZFE is approximated by:

$$u/u_o = \begin{cases} 1 & r < r_u \\ \exp\left[-\left(\dfrac{r - r_u}{b}\right)^2\right] & r \geq r_u \end{cases} \tag{4}$$

for a simple momentum jet.

Finally, the entrainment rate within the ZFE was shown to be

$$E/u_o r_o = 0.0204 + 0.00324(s/r_o) \tag{5}$$

for the simple momentum jet.

More recently, Sami, Carmody & Rouse[5] measured the axial and radial velocities, and some turbulence properties within the ZFE for the simple momentum jet. Their velocity profile measurements are in good agreement with equation 4. Kuethe[6] also measured the velocity profiles in this region.

Forstall & Shapiro[7] and Landis & Shapiro[8] studied momentum jets discharged to coflowing streams and deduced the length of the ZFE from their measurements. Their data were closely approximated by:

$$s_e/r_o = 8 + 24\ R \tag{6}$$

which shows that the starting length, s_e, increases with increasing velocity ratio, R. This expression is in conflict with Albertson's[4] measurements of s_e for R = 0.

Gordier,[9] Keffer & Baines,[10] and Platten & Keffer[11] measured the trajectories and centerline velocity decay for non-buoyant jets discharged normal to a cross flow. These data show that s_e decreases with increasing R.

Unfortunately, none of the above data indicate the values of centerline temperature or jet width at s_e. Further, no data exist describing the ZFE for buoyant jets discharged to either quiescent or flowing ambients.

Theoretical solutions for buoyant jet flows generally assume that the velocity and density (temperature, concentration) profiles normal to the jet axis are similar, i.e., the profiles are identical when plotted in appropriate coordinates. This is a reasonable assumption within the ZEF, but within the ZFE the profiles are definitely non-similar. At the diffuser exit the velocity and density profiles are "top-hat", i.e., the fluid is assumed to enter the environment as a plug flow while at the end of the ZFE the profiles are Gaussian; see figure 3. Within the ZFE the shape of the profiles gradually changes from top-hat to Gaussian, as shown in figure 4.

Theoretical solutions are currently limited to the ZEF. In order to define appropriate initial conditions for the ZEF, one must relate conditions at the diffuser exit to those at the end of the ZFE. Further, the length of the ZFE must also be determined.

Several methods are currently used to define these initial conditions. Hoult, et al.[12] and Platten & Keffer[11] ignore the ZFE, i.e., they assume it to be of zero length, and apply the diffuser exit conditions directly to their differential equations.

For buoyant jets discharged to quiescent ambients Fan[13] develops simple expressions for the jet radius and centerline density, based on the integrated forms of the momentum and energy equations. Fan neglects the effects of buoyancy and density stratification within the ZFE, and assumes that the length of the ZFE is 12.4 r_o regardless of buoyancy.

Based on Gordier's[9] data, Fan[13] develops similar expressions for s_e, θ_2, and b_e at the end of the ZFE for jets discharged to a cross flow. Fan's expressions contain many limitations, the most severe of which restricts them to flows in which the jet centerline remains in a single plane.

Abramovich[14] presents an expression for s_e for non-buoyant jets discharged to a coflowing stream. This expression shows that as R increases the length of the ZFE increases. Abramovich provides no relation for the centerline density at s_e.

Abraham[15-17] presents graphical solutions for the length of the region, within the ZFE, in which the centerline density remains constant. This length is shorter than the corresponding length for velocity because scalar properties diffuse more rapidly than momentum in free turbulent flows. This is shown in figure 4 where the velocity and temperature profiles within the ZFE are plotted; the temperature profile develops more rapidly than does the velocity profile. Abraham's solutions show that the starting length decreases with decreasing Froude number.

Thus, semi-empirical correlations exist which define s_e for non-buoyant jets discharged either parallel or perpendicular to a free stream. Similar expressions exist for buoyant jets discharged horizontally or vertically to quiescent ambients. But, these expressions do not cover the range of flows likely to occur with power plant thermal discharges. For example, existing methods are incapable of predicting s_e for jets discharged to stratified ambients, or for buoyant jets discharged to a free stream.

This report describes a theoretical method (based on previous ORNL research[3]) which can predict physical properties within the ZFE. These predictions can be used to define initial conditions for the ZEF methods.

Chapter 2 describes the new method. The integral equations, velocity, temperature and salinity profiles, and the entrainment function are developed and explained. The result is a set of six, non-linear, coupled ordinary differential equations, the solution to which provides values of r_u, r_t, r_c, b, Θ_1, and Θ_2 as functions of the streamwise coordinate, s.

Chapter 3 presents results obtained with this new method. Predictions of starting length are compared with the limited experimental data available and with the semi-empirical correlations proposed by Fan[13], Abramovich[14] and Abraham[16]. The parameters required for starting solutions within the ZEF are presented graphically for jets discharged with several Froude numbers at different velocity ratios: (1) horizontal and normal to the free stream, (2) vertically up, and (3) horizontal and parallel to the free stream.

In addition, the values of s_e as a function of Θ_{1o} and Θ_{2o} are shown for a particular Fr, R combination and the velocity and temperature profiles within the jet are computed for one case to show how the profiles develop within the ZFE. Finally, an example is given which shows how this method can be used to develop optimal discharge techniques for thermal effluents discharged through a single, circular, submerged diffuser.

Chapter 4 summarizes the pertinent features and limitations, and briefly discusses the results obtained with the new method.

2. Development of the Integral Method

This work is concerned with the behavior of momentum jets discharged to an infinite ambient through a single, circular, submerged diffuser. The jet is subjected to buoyancy forces, ambient cross flows and ambient density stratification. The basic equations governing the dynamics of the jet as it moves through the ambient are:

1. Conservation of mass
2. Conservation of energy
3. Conservation of salt (or any other scalar)
4. Conservation of momentum (3 scalar equations)

In order to derive a solvable system of equations the following assumptions are made:[3]

1. The flow is steady, in the mean.
2. The flow is fully turbulent; molecular diffusion is neglected.
3. The fluid is assumed incompressible; density variations are included only in the buoyancy terms.
4. All other fluid properties are assumed constant.
5. Fluid velocities are assumed low enough so that frictional heating can be neglected.
6. The pressure variation is assumed to be purely hydrostatic.
7. Changes in density are assumed to be small enough so that a linear equation of state is valid.
8. The flow within the jet is assumed to be axisymmetric.
9. The flow within the jet is assumed to be of boundary layer type, and the boundary layer approximations are valid.
10. The jet is discharged to an ambient fluid of infinite extent.
11. The ambient flow is laminar.

The coordinate system used in this analysis is shown in figure 5. x,y,z are the usual cartesian coordinates with z increasing vertically up and x,y forming the horizontal plane. The freestream velocity, u_∞, is assumed horizontal and parallel to the y axis.

s, r, ϕ are the coordinates in a "natural" curvilinear coordinate system. s measures the distance along the jet axis from the origin (diffuser exit); r is the radial distance from the jet axis; and the angle, ϕ, determines the orientation of r.

The two systems are related to each other by Θ_1 and Θ_2. Θ_1 measures the angle between the projection of the jet centerline onto the horizontal plane and the x axis. Θ_2 measures the angle between the jet centerline and the x,y plane.

Using this coordinate system and the assumptions listed earlier, the following ordinary differential equations[3] can be derived for buoyant jet flows:

continuity equation:

$$\frac{d}{ds}\int_0^\infty \bar{u}\, r\, dr = E \tag{7}$$

energy equation:

$$\frac{d}{ds}\int_0^\infty \bar{u}\,(\bar{t} - t_\infty)\,r\,dr = -\frac{dt_\infty}{ds}\int_0^\infty \bar{u}\,r\,dr \tag{8}$$

concentration equation:

$$\frac{d}{ds}\int_0^\infty \bar{u}\,(\bar{c} - \bar{c}_\infty)\,r\,dr = -\frac{dc_\infty}{ds}\int_0^\infty \bar{u}\,r\,dr \tag{9}$$

s-momentum (parallel to jet axis) equation:

$$\frac{d}{ds}\int_0^\infty \bar{u}^2\,r\,dr = \int_0^\infty \frac{\rho_\infty - \bar{\rho}}{\rho_o}\,r\,dr\,g\,S_2 + E\,u_\infty\,S_1C_2 \tag{10}$$

$\bar{k}$-momentum (vertical) equation:

$$\frac{d}{ds}\left[\int_0^\infty \bar{u}^2\,r\,dr\right]S_2 = \int_0^\infty \frac{\rho_\infty - \bar{\rho}}{\rho_o}\,r\,dr\,g - q\,C_2\,\frac{d\Theta_2}{ds} \tag{11}$$

$\bar{j}$-momentum (parallel to free stream) equation:

$$\frac{d}{ds}\left[\int_0^\infty \bar{u}^2\,r\,dr\right]S_1C_2 = E\,u_\infty - q\left[C_1C_2\,\frac{d\Theta_1}{ds} - S_1S_2\,\frac{d\Theta_2}{ds}\right] \tag{12}$$

Equations (11) and (12) can be simplified using equation (10) to yield:

$$\frac{d\Theta_1}{ds} = \frac{E\,u_\infty\,C_1}{q\,C_2} \tag{13}$$

$$\frac{d\Theta_2}{ds} = \frac{\int_0^\infty \frac{\rho_\infty - \bar{\rho}}{\rho_o}\,r\,dr\,g\,C_2 - E\,u_\infty\,S_1S_2}{q} \tag{14}$$

where

$$q = \int_0^\infty \bar{u}^2 \, r \, dr - \frac{1}{4} E^2$$

The density can be written in terms of the temperature and salinity as[3]:

$$\frac{\bar{\rho} - \rho_\infty}{\rho_o} = \beta(t_\infty - \bar{t}) + \gamma(c_\infty - \bar{c}) \tag{15}$$

The cartesian coordinates of the jet centerline (x,y,z) can be expressed in terms of s, θ_1, and θ_2 as follows[3]:

$$x = \int_0^s C_1 \, C_2 \, ds \qquad y = \int_0^s S_1 \, C_2 \, ds \qquad z = \int_0^s S_2 \, ds \tag{16}$$

These equations can be non-dimensionalized by normalizing all the variables on the jet properties at the diffuser exit – u_o, r_o, t_o, c_o, and ρ_o. Writing the equations in this form introduces three non-dimensional parameters – R, Fr, and T. The velocity ratio, R, is the ratio of free stream velocity to initial jet velocity. The Froude number, Fr, is the ratio of inertia to buoyancy forces. The stratification parameter, T, is the ratio of initial density difference to ambient density gradient.

In order to solve equations (7) – (10), (13), and (14) the velocity, temperature, and concentration profiles normal to the jet axis must be specified. The velocity profile suggested by Albertson, et al.,[4] equation (4), is limited in applicability. For jets discharged to a flowing stream, the longitudinal velocity (parallel to the jet axis) far from the jet axis will be u_{12} (= $u_\infty S_1 C_2$). Generalizing equation (4) to jets discharged to flowing streams gives:

$$\bar{u} = \begin{cases} u_o & r < r_u \\ \Delta u_o \exp\left[-\left(\dfrac{r - r_u}{b}\right)^2\right] + u_{12} & r \geq r_u \end{cases} \tag{17}$$

where $\Delta u_o = u_o - u_{12}$.

Similarly, the temperature profile is assumed to be:

$$\Delta\bar{t}/\Delta t_o = \begin{cases} 1 & r < r_t \\ \exp\left[-\left(\dfrac{r - r_t}{\lambda b}\right)^2\right] & r \geq r_t \end{cases} \tag{18}$$

and the concentration profile is assumed to be:

$$\Delta\bar{c}/\Delta c_o = \begin{cases} 1 & r < r_c \\ \exp\left[-\left(\dfrac{r - r_c}{\lambda b}\right)^2\right] & r \geq r_c \end{cases} \tag{19}$$

In the above equations, r_u, r_t, and r_c are the potential core widths for velocity, temperature, and salinity, respectively. The widths for temperature and salinity are unequal only for stratified flows. b is a measure of the width of the free-turbulent (jet) flow for velocity and λb is the corresponding width for the scalar profiles.

These profiles introduce four unknowns – r_u, r_t, r_c, and b. The angles θ_1 and θ_2 provide two additional unknowns for a total of six dependent variables – equal to the number of equations.

These profiles are substituted into the integrals appearing in the differential equations, as shown in Appendix A. In order to evaluate the integrals involving both the velocity and temperature (or concentration), for example:

$$\int_0^\infty \bar{u}\,(\bar{t} - t_\infty)\, r\, dr,$$

we assume that $r_u = r_t$ (or r_c). Without this simplification, these integrals are quite difficult to evaluate. However, the approximation will yield accurate values for these integrals except (perhaps) near the end of the ZFE. In any case, this approximation is less critical than are the entrainment assumptions made later in the chapter.

In Appendix B the governing differential equations are written in terms of the integrals developed in Appendix A. As shown in Figure 6, there are two distinct regions within the ZFE. In the first region r_u, r_t, and r_c are all greater than zero. Since scalar properties diffuse more rapidly in a free-turbulent flow than do vector properties, the centerline temperature and salinity will begin to decrease from their diffuser outfall values before the end of the velocity potential core is reached.

The second region is downstream of the point where r_t (or r_c) becomes zero. Beyond this point, r_t and r_c are required to remain zero and the new dependent variables are t_m and c_m which now decay from their initial values.

Thus, in region 1, the differential equations can be written as:

$$\begin{bmatrix} a_{11} & o & o & a_{14} \\ o & a_{22} & o & a_{24} \\ o & o & a_{33} & a_{34} \\ a_{41} & o & o & a_{44} \end{bmatrix} \begin{bmatrix} r_u' \\ r_t' \\ r_c' \\ b' \end{bmatrix} = \begin{bmatrix} f_1 \\ f_2 \\ f_3 \\ f_4 \end{bmatrix}$$

$$\Theta_1' = f_5 \qquad \Theta_2' = f_6 \tag{20}$$

where the a_{ij} and the f_i are defined in Appendix B, equation (B-11).

In region 2, the differential equations are:

$$\begin{bmatrix} A_{11} & o & o & A_{14} \\ o & A_{22} & o & A_{24} \\ o & o & A_{33} & A_{34} \\ A_{41} & o & o & A_{44} \end{bmatrix} \begin{bmatrix} r_u' \\ \Delta t_m' \\ \Delta c_m' \\ b' \end{bmatrix} = \begin{bmatrix} F_1 \\ F_2 \\ F_3 \\ F_4 \end{bmatrix}$$

$$\Theta_1' = F_5 \qquad \Theta_2' = F_6 \tag{21}$$

where the coefficients are defined in equation (B-12).

In order to achieve closure the entrainment rate, E, must be specified. Albertson's correlation for E, equation (5), is valid only for the simple momentum jet. Using equation (3), equation (5) can be rewritten as:

$$E/u_o r_o = 0.0204 + 0.0284\ (b/r_o) \tag{22}$$

In reference 3, a general expression for the entrainment rate in the zone of established flow was developed, based on the works of Hoult, et al.[12] and Fox.[18] The entrainment function used there is:

$$E = \left(a_1 + \frac{a_2}{Fr} S_2\right)\left[u_m b \mid 1 - R_{12} \mid + a_3 u_\infty b \sqrt{1 - (S_1 C_2)^2}\right] \tag{23}$$

In order to develop an entrainment equation valid for a wide range of flows within the ZFE we shall assume that the form of equation (23) is valid within the ZFE. This assumption, plus the requirement that the entrainment equation reduce to equation (22) for simple momentum jets, suggests the following entrainment function for the ZFE:

$$E/u_o r_o = \left[0.0204 + 0.0284(b/r_o)\right]\left[1.0 + \frac{A_2}{Fr} S_2\right]$$
$$\times \left[\mid 1 - R_{12} \mid + A_3 R \sqrt{1 - (S_1 C_2)^2}\right] \tag{24}$$

Equation (24) appears to account for the important factors which influence entrainment – jet width, b; buoyancy, Fr; jet orientation, θ_1 and θ_2; and the free stream velocity, R.

Lack of sufficient experimental data within the ZFE prohibit a more scientific development of the entrainment function. However, as we shall later see, the predictions obtained with this function appear reasonable and are in reasonable agreement with the limited data available. As more data are obtained, a more accurate function can be developed. Even then, the equations and profiles used here will still provide the framework needed to predict jet development within the ZFE.

Equations (20), (21), and (24) have been programmed for the IBM 360 computer using FORTRAN IV. Hamming's modified predictor-corrector method (IBM Scientific Subroutine Package HPCG)[19] is used to numerically solve the differential equations. The initial conditions include the potential core widths ($r_u = r_t = r_c = 1$), turbulent jet width ($b = 0$), and initial angles, Θ_1 and Θ_2. The values of Fr, R, and T must also be specified. The solution then proceeds by marching in the direction of increasing s.

3. Results Obtained With the Method

Equations (20), (21), and (24) are sufficient to determine jet development within ZFE. However, the coefficients in the entrainment equation (24) must be determined first.

For the simple momentum jet (i.e., $Fr = \infty$, $R = 0$) equation (24) reduces to equation (22). Predictions made with this entrainment function give a value of s_e/r_o greater than the 12.4 measured by Albertson, et al.[4] Increasing the constants in equation (22) by 5% bring the predictions closely in line with experimental data for the simple momentum jet. Therefore, all further predictions are made with these coefficients so increased.

The predictions for the simple momentum jet are compared with experimental velocity profiles obtained by Sami, et al.,[5] in figure 7. The agreement between theory and experiment is excellent throughout the ZFE.

The coefficient A_3 determines the influence of cross flows on the entrainment. Its value was determined by fitting the present predictions with Gordier's[9] data and Fan's[13] correlation of that data, which can be written as:

$$s_e/r_o = 12.4\ e^{-3.4R} \tag{25}$$

valid for non-buoyant jets discharged to a cross flow. Predictions made with $A_3 = 4.3$ give good agreement with Gordier's data and Fan's correlation; see figure 8. Starting length values measured by Platten & Keffer[11] are also shown on the figure. These values are considerably lower than those measured by Gordier, but no obvious explanation exists for this discrepancy.

The method, with A_2 unspecified, is now capable of predicting all non-buoyant jet flows. Figure 9 shows the present predictions and the correlation given by Abramovich,[14] equation (26), for non-buoyant jets discharged to a coflowing stream:

$$s_e/r_o = 12.4 \left|\frac{1 + R}{1 - R}\right| \frac{1}{\sqrt{1 + 1.18\ R}} \tag{26}$$

where Abramovich's constants were adjusted so that $s_e/r_o = 12.4$ when $R = 0$. Also shown are the experimental measurements obtained by Shapiro, et al.[7,8] The agreement between the present method and the Abramovich correlation is remarkably good. The new method predicts values of s_e which are higher than those measured by Shapiro, but the agreement is qualitatively satisfactory. Hinze[20] questioned the accuracy of this data since it seems to conflict with the value $s_e/r_o = 12.4$ for $R = 0$.

The coefficient, A_2, determines the influence of initial buoyancy on the entrainment. Its value was determined by fitting the present predictions with Abraham's[16] correlations for horizontal and vertical buoyant jets discharged to quiescent ambients. Predictions made with $A_2 = 34$ give satisfactory agreement with Abraham's correlations; see figure 10. Unfortunately, no data within the ZFE exist for buoyant jets so it is impossible to empirically check the accuracy of this method for buoyant jet flows.

The entrainment equation used in all further calculation is:

$$E/u_o r_o = 1.05 \left[0.0204 + 0.0284(b/r_o)\right]\left[1.0 + \frac{34}{Fr} S_2\right]$$

$$\times \left[\left|1 - R_{12}\right| + 4.3\ R \sqrt{1 - (S_1 C_2)^2}\right] \tag{27}$$

This method is now capable of predicting development within the ZFE for buoyant jets discharged at arbitrary angles to flowing, stratified ambients.

Figures 11-15 present the predictions of s_e/r_o, b_e/r_o, $\Delta t_e/\Delta t_o$, θ_{1e}, θ_{2e} for jets discharged horizontally and normal to the free stream for several values of Fr and R. As the free stream velocity increases, the starting length, jet width, and θ_{2e} decrease while the centerline temperature and θ_{1e} increase. As the jet becomes more buoyant (Fr decreases) the

starting length and centerline temperature decrease, while the jet width and angles increase.

Figures 16–19 present similar predictions for jets discharged vertically up. For these flows (with $\Theta_2 = 90°$) Θ_1 is undefined and the Θ_1 equation does not enter into the calculations. The effects of R and Fr are very similar to those for jets discharged horizontally and perpendicular to the free stream. The curves for Fr = 5 in figures 16–18 are unexpected because they are not monotonically increasing (or decreasing).

Figures 20–23 present predictions for jets discharged horizontally and parallel to the free stream. When the velocity ratio is 1.0, the jet and free stream are moving at the same velocity so there is no jet, which accounts for the discontinuities at R = 1.0 on these figures. These figures show that the influence of a coflowing stream is the reverse of that from a cross flow. The results for Fr = 5 are not shown here because numerical instabilities which appeared in those calculations reduce confidence in those results. The low Fr curves on figures 20–22 are unusual because they cross over the higher Fr curves.

The anomolies in figures 16–18 and 20–22 suggest that the low Froude number results presented here be used with caution. These anomolies may be due to an inaccurate entrainment function; unfortunately the validity of equation (24) at low Fr cannot be checked because no experimental data for the ZFE of buoyant jets exist. Alternatively, these anomolies may appear because the velocity within the potential core increases at low Froude numbers* due to the buoyancy driven acceleration. This analysis would therefore be invalid for these Froude numbers. In particular, equation (17) would have to be modified.

Because of the different influences of the ambient flow, according to whether the jet is perpendicular or parallel to the free stream, we compute the starting length for a variety of Θ_1, Θ_2 values with Fr and R fixed. The results of this computation are shown in figure 24 for a jet discharged with Fr = 40 and R = 0.2. The starting length increases with increasing Θ_1 and decreasing Θ_2.

---

*$Fr < O(1)$.

Figure 4 shows how the jet develops for a particular set of initial conditions. The jet shown is discharged horizontally to a quiescent ambient with an initial Froude number of 40. The jet curves upward due to the buoyancy force. The turbulence and entrainment at the edge of the jet diffuse the jet outward, as shown by the growth in jet width, b. Velocity and temperature profiles are shown at four stations within the ZFE. Initially, the profiles are top-hat, but as we move downstream the profiles become more nearly Gaussian. Note that the temperature profile decays more rapidly than does the velocity profile.

This method can be used to help design optimum systems for power plant thermal effluents discharged through a single, submerged, round diffuser. For example, for a jet discharged with Fr = 40 and R = 0.2 (figure 24) Table 1 shows the size of the region within which the temperature is equal to the diffuser exit temperature, i.e., $t(r,s) = t_o$. This table shows that the size of this maximum temperature region is roughly proportional to the length of the mixing zone. Thus, as shown in figure 24, discharging the jet vertically up will reduce the extent of this mixing zone. Also, jets discharged perpendicular to the ambient, rather than parallel to the ambient, yield smaller mixing zones. These results have been confirmed by calculations within the zone of established flow.[3]

Table 1. Mixing Zone Size As A Function Of Initial Orientation

θ_{1_o}	θ_{1_o}	V^a
0°	0°	1.0
30	0	1.05
60	0	1.29
90	0	1.71
0	30	0.825
30	30	0.873
60	30	1.01
90	30	1.12
0	60	0.733
30	60	0.759
60	60	0.785
90	60	0.802
--	90	0.706

$$^a V = \frac{\text{Volume within which } t = t_o}{\text{Corresponding volume at } 0°, 0°}$$

4. Summary

The method developed in chapter 2 uses the integral conservation equations of mass, energy, concentration, and momentum. A modified Gaussian is used to evaluate the velocity, temperature, and salinity profiles and a new entrainment function is postulated. The result is a set of six, non-linear, coupled, ordinary differential equations, the solution to which includes the length of the zone of flow establishment; and values of centerline temperature, salinity, jet width, and jet orientation. The method is quite general, capable of predicting buoyant jets discharged to flowing, stratified ambients (three-dimensional trajectory flows).

However, the method is limited to steady flows for which the free stream is laminar. Further, the accuracy of the new entrainment function can be determined only after additional experimental data become available. Therefore, predictions obtained with this method should be used cautiously. This is particularly true for low Froude number flows where the method may not be valid.

There is a real need for more velocity and temperature profile measurements within the ZFE. To date, only the ZFE of the simple momentum jet has been extensively studied, while the ZFE of buoyant jets has been completely ignored.

Predictions have been compared with the limited experimental data available for non-buoyant jets and the agreement is adequate. The agreement between present predictions and the Fan,[13] Abramovich,[14] and Abraham[16] correlations is quite good.

The output of this method can be used to define the initial conditions required for the conventional Zone of Established Flow methods. These initial conditions are presented graphically in figures 11–23 for three different initial jet orientations. Coupling these initial conditions with conventional methods should provide more accurate predictions of jet development.

This is particularly important for thermal plumes from power plants, where one is primarily concerned with the region near the outfall in which the temperature excess is large. This method provides, for the first time, predictions of the size and location of this zone and the temperature field within this zone, for thermal effluents discharged through single, circular, submerged diffusers.

References

1. D. J. Baumgartner & D. S. Trent, Ocean Outfall Design Part I: Literature Review and Theoretical Development, U. S. Department of Interior, Federal Water Quality Administration, 1970.

2. E. Silberman & H. Stefan, Physical (Hydraulic) Modeling of Heat Dispersion in Large Lakes, A Review of the State of the Art, U. Of Minn., St. Anthony Falls Hydraulic Lab., Project Report No. 115, 1970.

3. E. Hirst, Analysis of Round, Turbulent, Buoyant Jets Discharged to Flowing, Stratified Ambients, ORNL Rep. 4685, Oak Ridge National Lab., 1971.

4. M. L. Albertson, Y. B. Dai, R. A. Jensen, & H. Rouse, "Diffusion of Submerged Jets," ASCE Trans., 115, 639–697, 1950.

5. S. Sami, T. Carmody & H. Rouse, "Jet Diffusion in the Region of Flow Establishment," J. Fluid Mech., 27, 2, 231–252, 1967.

6. A. M. Kuethe, "Investigations of the Turbulent Mixing Regions Formed by Jets," J. Applied Mech., 2, A, 1935.

7. W. Forstall & A. H. Shapiro, "Momentum and Mass Transfer in Co-axial Gas Jets," J. Appl. Mech., 17, 399–408, 1950.

8. F. Landis, & A. H. Shapiro, "The Turbulent Mixing of Co-axial Gas Jets," Heat Trans. & Fluid Mech. Inst., 1951.

9. R. L. Gordier, Studies of Fluid Jets Discharging Normally into Moving Liquid, U. of Minn., St. Anthony Falls Hydraulic Lab., Tech. Paper No. 28, Series B, 1959.

10. J. F. Keffer & W. D. Baines, "The Round Turbulent Jet in a Cross-Wind," J. Fluid Mech., 15, 4, 481–497, 1963.

11. J. L. Platten & J. F. Keffer, Entrainment in Deflected Axisymmetric Jets at Various Angles to the Stream, U. Toronto, Mech. Engineering Dept., UTME-TP-6808, 1968.

12. D. P. Hoult, J. A. Fay & L. J. Forney, "A Theory of Plume Rise Compared with Field Observations," J. Air Pollution Control Association, 19, 9, 585–590, 1969.

13. L. N. Fan, Turbulent Buoyant Jets into Stratified or Flowing Ambient Fluids, Keck Lab. of Hydraulics and Water Resources, CIT, Rep. No. KH-R-15, 1967.

14. G. N. Abramovich, The Theory of Turbulent Jets, Translation by Scripta Technica, MIT Press, 1963.

15. G. Abraham, "Jet Diffusion in Liquid of Greater Density," ASCE J. Hydraulics Div., 86, HY6, 1–13, 1960.

16. G. Abraham, Jet Diffusion in Stagnant Ambient Fluid, Delft Hydraulics Laboratory, No. 29, 1963.

17. G. Abraham, "Horizontal Jets in Stagnant Fluid of Other Density," ASCE J. Hydraulics Div., 91, HY4, 139–153, 1965.

18. D. G. Fox, "Forced Plume in a Stratified Fluid," J. Geophysical Res., 75, 33, 6818–6835, 1970.

19. System/360 Scientific Subroutine Package, H20-0205-3, 4th Edition, IBM, 1968.

20. J. O. Hinze, Turbulence, McGraw-Hill Book Company, 1959.

APPENDIX A

Evaluation of the Integrals In the Differential Equations

The differential equations, (7) - (10), (13) and (14), contain several integrals which involve the velocity, temperature, and concentration profiles, equations (17) - (19). In this Appendix, the integrals are evaluated using these profiles.

Equation (7) contains the mass flux integral, denoted by I_1, which is:*

$$I_1 = \int_0^\infty \bar{u}\, r\, dr = \int_0^{r_u} u_o\, r\, dr + \int_{r_u}^\infty \Delta u_o\, e^{-\left(\frac{r - r_u}{b}\right)^2} r\, dr + \int_{r_u}^{r_u + \sqrt{2}\, b} u_{12}\, r\, dr \tag{A-1}$$

$$I_1 = \frac{1}{2} u_o\, r_u^2 + \left[u_o \frac{\sqrt{\pi}}{2} + \left(\sqrt{2} - \frac{\sqrt{\pi}}{2}\right) u_{12}\right] r_u\, b + (u_o + u_{12}) \frac{b^2}{2} \tag{A-2}$$

Equation (8) contains the energy flux integral, I_2, which is:

$$I_2 = \int_0^\infty \bar{u}(\bar{t} - t_\infty)\, r\, dr \cong \int_0^{r_t} \Delta t_o\, u_o\, r\, dr + \int_{r_t}^\infty \Delta t_o\, e^{-\left(\frac{r - r_t}{\lambda b}\right)^2} \times \left[\Delta u_o\, e^{-\left(\frac{r - r_t}{b}\right)^2} + u_{12}\right] r\, dr \tag{A-3}$$

The difference between r_u and r_t is ignored in evaluating I_2. An exact solution is impossible without this assumption. In actuality, r_u and r_t

---

*The outer edge of the jet is taken as $r_u + \sqrt{2}\, b$ for the integrals involving $u_{12} - I_1$ and I_4.

are very nearly equal, except in the region where r_t is zero; see figure 6.

$$I_2 = \Delta t_o \left[\frac{1}{2} u_o r_t^2 + b\, r_t \left(\frac{u_o - u_{12}}{\sqrt{\lambda^2 + 1}} + u_{12} \right) \frac{\lambda \sqrt{\pi}}{2} \right.$$

$$\left. + b^2 \left(\frac{u_o - u_{12}}{\lambda^2 + 1} + u_{12} \right) \frac{\lambda^2}{2} \right] \qquad \text{(A-4)}$$

The integral on the left hand side of equation (9) is identical to I_2, with t replaced by c. This integral, denoted by I_3, is:

$$I_3 = \int_o^\infty \bar{u}\, (\bar{c} - c_\infty)\, r\, dr$$

$$= \Delta c_o \left[\frac{1}{2} u_o r_c^2 + b\, r_c \left(\frac{u_o - u_{12}}{\sqrt{\lambda^2 + 1}} + u_{12} \right) \frac{\lambda \sqrt{\pi}}{2} \right.$$

$$\left. + b^2 \left(\frac{u_o - u_{12}}{\lambda^2 + 1} + u_{12} \right) \frac{\lambda^2}{2} \right] \qquad \text{(A-5)}$$

Once again, the widths of the velocity and salinity potential cores are assumed identical, i.e., $r_c = r_u$.

The momentum equation (10) contains the momentum flux integral, denoted by I_4:

$$I_4 = \int_o^\infty u^2\, r\, dr = \int_o^{r_u} u_o^2\, r\, dr + \int_{r_u}^\infty \left[(\Delta u_o)^2\, e^{-2\left(\frac{r - r_u}{b}\right)^2} \right.$$

$$\left. + 2u_{12}\, \Delta u_o\, e^{-\left(\frac{r - r_u}{b}\right)^2} \right] r\, dr + \int_{r_u}^{\sqrt{2}\, b + r_u} u_{12}^2\, r\, dr \qquad \text{(A-6)}$$

$$I_4 = \frac{1}{2} u_o^2 r_u^2 + r_u b \left[\left(\frac{\sqrt{\pi}}{2\sqrt{2}} \right) u_o^2 + u_o u_{12} \left(\sqrt{\pi} - \frac{\sqrt{\pi}}{\sqrt{2}} \right) \right.$$

$$\left. + u_{12}^2 \left(\frac{\sqrt{\pi}}{2\sqrt{2}} - \sqrt{\pi} + \sqrt{2} \right) \right] + \frac{b^2}{4} (u_o + u_{12})^2 \qquad \text{(A-7)}$$

The momentum equation (10) also contains the integral of density - difference, denoted by I_5. This integral can be evaluated using the equation of state (15) and the temperature and salinity profiles, equations (18) and (19):

$$I_5 = \int_o^\infty \frac{\rho_\infty - \bar{\rho}}{\rho_o} r \, dr = \beta \int_o^\infty (\bar{t} - t_\infty) \, r \, dr + \gamma \int_o^\infty (\bar{c} - c_\infty) \, r \, dr \qquad \text{(A-8)}$$

$$I_5 = \beta \, \Delta t_o \left[\frac{r_t^2}{2} + \frac{\lambda^2 b^2}{2} + \frac{\sqrt{\pi}}{2} \lambda \, b \, r_t \right]$$

$$+ \gamma \, \Delta c_o \left[\frac{r_c^2}{2} + \frac{\lambda^2 b^2}{2} + \frac{\sqrt{\pi}}{2} \lambda \, b \, r_c \right] \qquad \text{(A-9)}$$

APPENDIX B

Evaluation of the Differential Equations

The integrals, evaluated in Appendix A, can now be substituted into the differential equations (7) – (10), (13), and (14). In order to reduce the algebraic complexity, we assume that, locally, the values of Θ_1 and Θ_2 remain constant. That is, the rates of change of the terms involving Θ_1 and Θ_2 are assumed to be much smaller than the rates of change of the terms involving b, r_u, r_t and r_c in the conservation of mass, energy, concentration, and s-momentum equations. In the last two momentum equations (13) and (14) the derivatives of Θ_1 and Θ_2 are, of course, not neglected.

We make certain definitions for later use:

$$d_1 = u_o \frac{\sqrt{\pi}}{2} + \left(\sqrt{2} - \frac{\sqrt{\pi}}{2}\right) u_{12}$$

$$d_2 = \left(\frac{u_o - u_{12}}{\sqrt{\lambda^2 + 1}} + u_{12}\right) \frac{\lambda\sqrt{\pi}}{2}$$

$$d_3 = \left(\frac{u_o - u_{12}}{\lambda^2 + 1} + u_{12}\right) \lambda^2$$

$$d_4 = u_o^2 \frac{\sqrt{\pi}}{2\sqrt{2}} + u_o u_{12} \left(\sqrt{\pi} - \frac{\sqrt{\pi}}{\sqrt{2}}\right) + u_{12}^2 \left(\frac{\sqrt{\pi}}{2\sqrt{2}} - \sqrt{\pi} + \sqrt{2}\right)$$

$$d_5 = \frac{1}{2} (u_o + u_{12})^2$$

Now the integrals from Appendix A, and the d_i can be substituted into the differential equations to yield:

continuity equation (7):

$$(u_o r_u + b\, d_1)\, r_u' + \left[d_1 r_u + (u_o + u_{12})\, b\right] b' = E \qquad \text{(B-2)}$$

energy equation (8):

$$(u_o r_t + d_2 b)\, r_t' + (d_2 r_t + d_3 b)\, b'$$

$$= \frac{dt_\infty}{ds}\left(-I_1 + \frac{1}{2}\, u_o r_t^2 + r_t b\, d_2 + \frac{1}{2}\, b^2 d_3\right) / \Delta t_o \qquad \text{(B-3)}$$

concentration equation (9):

$$(u_o r_c + d_2 b)\, r_c' + (d_2 r_c + d_3 b)\, b'$$

$$= \frac{dc_\infty}{ds}\left(-I_1 + \frac{1}{2}\, u_o r_c^2 + r_c b\, d_2 + \frac{1}{2}\, b^2 d_3\right) / \Delta c_o \qquad \text{(B-4)}$$

s-momentum equation (10):

$$(u_o^2 r_u + d_4 b)\, r_u' + (d_5 b + d_4 r_u)\, b' = I_5 g\, S_2 + E\, u_{12} \qquad \text{(B-5)}$$

Θ_1-equation (13):

$$\Theta_1' = \frac{E\, u_\infty C_1}{q\, C_2} \qquad \text{(B-6)}$$

Θ_2-equation (14):

$$\Theta_2' = \frac{I_5 g\, C_2 - E\, u_\infty S_1 S_2}{q} \qquad \text{(B-7)}$$

where $q = I_4 - E^2/4$, $\Delta t_o = t_o - t_\infty(z)$, $\Delta c_o = c_o - c_\infty(z)$, and $(\ )' = d(\ )/ds$.

Equations (B-2) – (B-7) are valid only for $r_u > 0$, $r_t > 0$, and $r_c > 0$. Once any of these potential core widths becomes zero, these equations are no longer appropriate. Beyond that point, the centerline temperature (or concentration) will decay from its initial value,

t_o (or c_o). Also, the potential core width will remain zero, $r_t = 0$ (or $r_c = 0$). Thus t_m (or c_m) becomes a dependent variable replacing r_t (or r_c).

In the portion of the ZFE beyond where $r_t = 0$, the energy and concentration equations are changed, as is the density-difference integral, I_5.

The energy equation (B-3) becomes:

$$\left(\frac{b^2}{2} d_3\right) \Delta t_m' + \Delta t_m \, b \, d_3 \, b' = \frac{-dt_\infty}{ds} I_1 \qquad \text{(B-8)}$$

Similarly, the concentration equation (B-4) becomes:

$$\left(\frac{b^2}{2} d_3\right) \Delta c_m' + \Delta c_m \, b \, d_3 \, b' = \frac{-dc_\infty}{ds} I_1 \qquad \text{(B-9)}$$

And finally, the density-difference integral becomes:

$$I_5 = (\Delta t_m \, \beta + \Delta c_m \, \gamma) \frac{\lambda^2 b^2}{2} \qquad \text{(B-10)}$$

where $\Delta t_m = t_m - t_\infty(z)$ and $\Delta c_m = c_m - c_\infty(z)$.

So, in the region where $r_t = 0$ and $r_u > 0$ the governing differential equations are (B-2), (B-8), (B-9), and (B-5) – (B-7), with equation (B-10) substituted for the definition of I_5 from equation (A-9).

The governing equations for both regions within the ZFE can be written in matrix form, as shown in Chapter 2. The coefficients in equation (20) are:

$$a_{11} = u_o r_u + b \, d_1$$

$$a_{14} = d_1 r_u + (u_o + u_{12}) \, b$$

$$f_1 = E$$

$$a_{22} = u_o r_t + d_2 b$$

$$a_{24} = d_2 r_t + d_3 b$$

$$f_2 = \frac{dt_\infty}{ds}\left(-I_1 + \frac{1}{2} u_o r_t^2 + r_t b\ d_2 + \frac{1}{2} b^2 d_3\right) / \Delta t_o$$

$$a_{33} = u_o r_c + d_2 b$$

$$a_{34} = d_2 r_c + d_3 b$$

$$f_3 = \frac{dc_\infty}{ds}\left(-I_1 + \frac{1}{2} u_o r_c^2 + r_c b\ d_2 + \frac{1}{2} b^2 d_3\right) / \Delta c_o$$

$$a_{41} = u_o^2\ r_u + d_4 b$$

$$a_{44} = d_5 b + d_4 r_u$$

$$f_4 = I_5\ g\ S_2 + E\ u_{12}$$

$$f_5 = \frac{E\ u_\infty C_1}{q\ C_2}$$

$$f_6 = \frac{I_5\ g\ C_2 - E\ u_\infty\ S_1 S_2}{q} \qquad \text{(B-11)}$$

The coefficients in equation (21) are:

$$A_{11} = a_{11}$$

$$A_{14} = a_{14}$$

$$F_1 = f_1$$

$$A_{22} = b^2 \; d_3/2$$

$$A_{24} = \Delta t_m \; b \; d_3$$

$$F_2 = \frac{-d \; t_\infty}{ds} \; I_1$$

$$A_{33} = b^2 \; d_3/2$$

$$A_{34} = \Delta c_m \; b \; d_3$$

$$F_3 = \frac{-d \; c_\infty}{ds} \; I_1$$

$$A_{41} = a_{41}$$

$$A_{44} = a_{44}$$

$$F_4 = f_4$$

$$F_5 = f_5$$

$$F_6 = f_6 \qquad \text{(B-12)}$$

with I_5 (in f_4 and f_6) changed to:

$$I_5 = (\Delta t_m \beta + \Delta c_m \gamma) \; \lambda^2 b^2/2$$

APPENDIX C

FIGURES

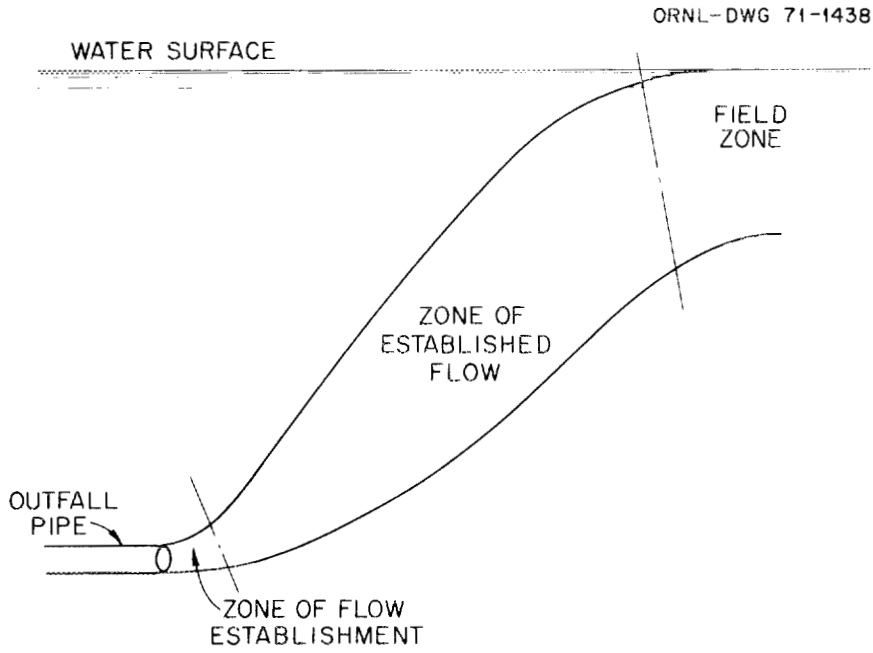

Fig. 1. Flow Regimes for Buoyant Jets.

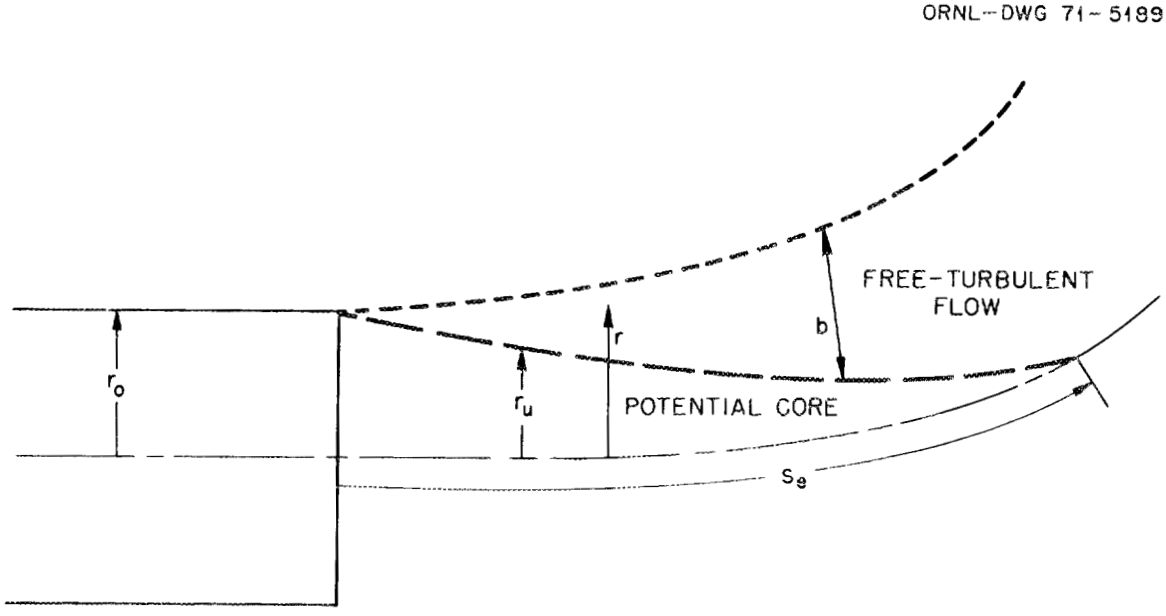

Fig. 2. Schematic Representation of the Zone of Flow Establishment.

ORNL-DWG 71-1437

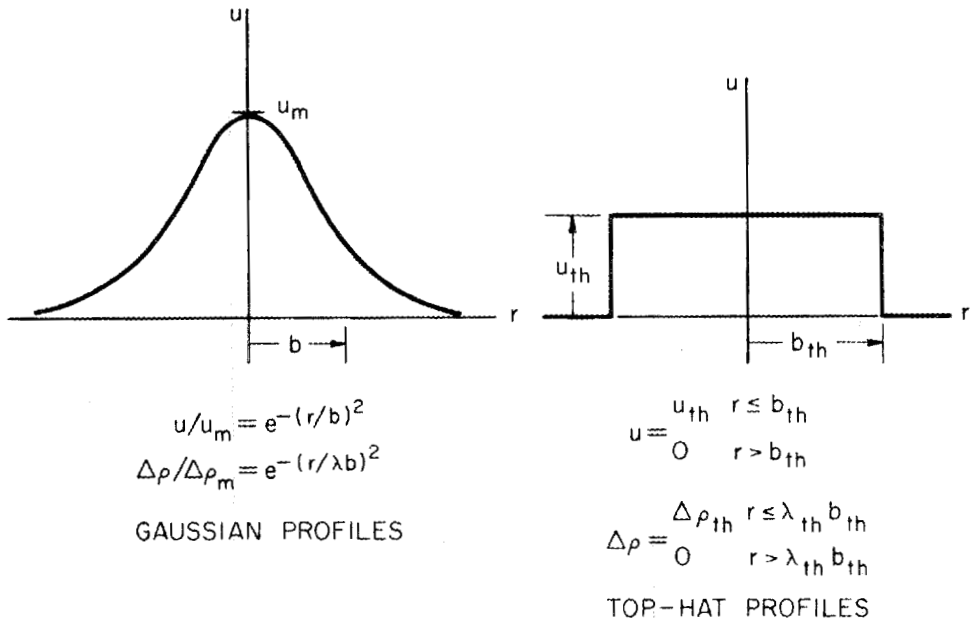

Fig. 3. Velocity and Density-Difference Profile Shapes.

ORNL-DWG 71-5188

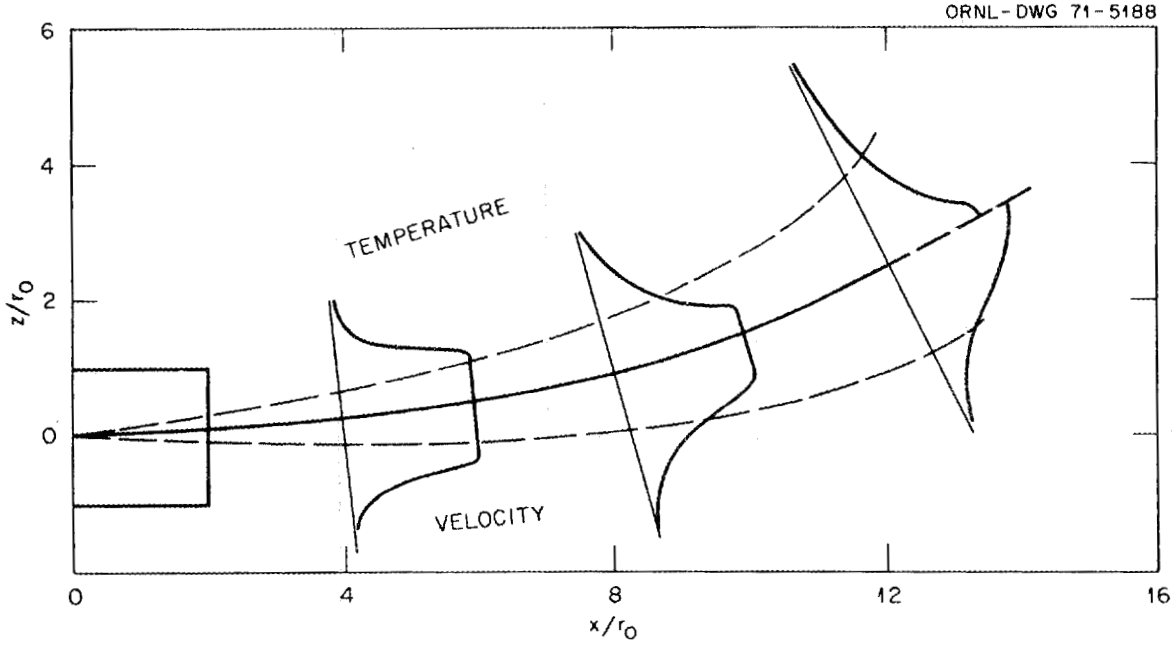

Fig. 4. Velocity and Temperature Profiles Within the Zone of Flow Establishment. Jet is Discharged with Fr = 40, R = 0, $\Theta_{1_0} = 0°$, $\Theta_{2_0} = 0°$.

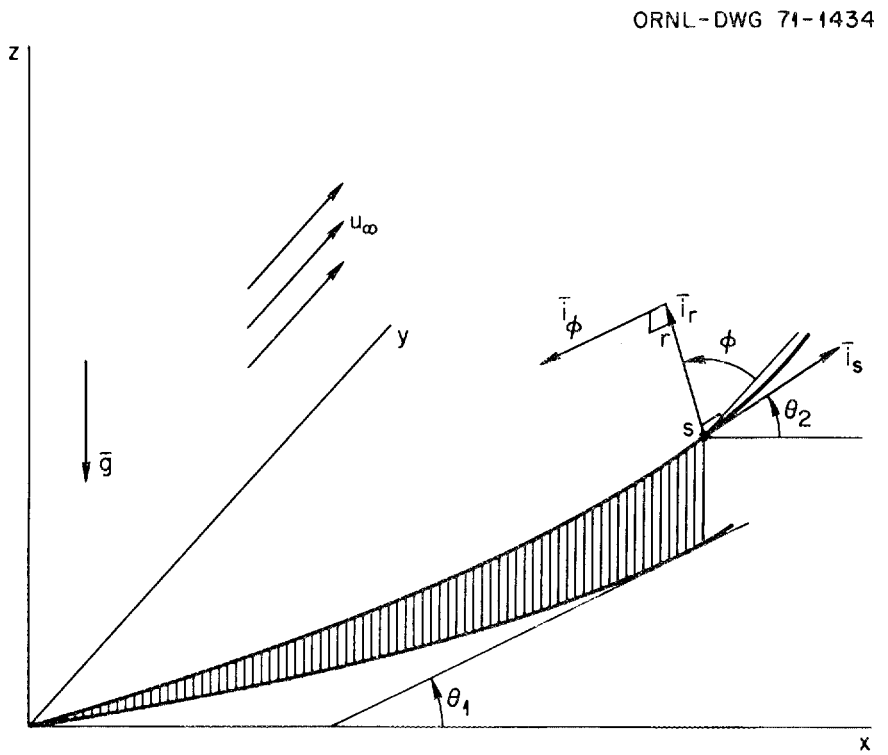

Fig. 5. Natural Coordinate System for Buoyant Jet Analysis.

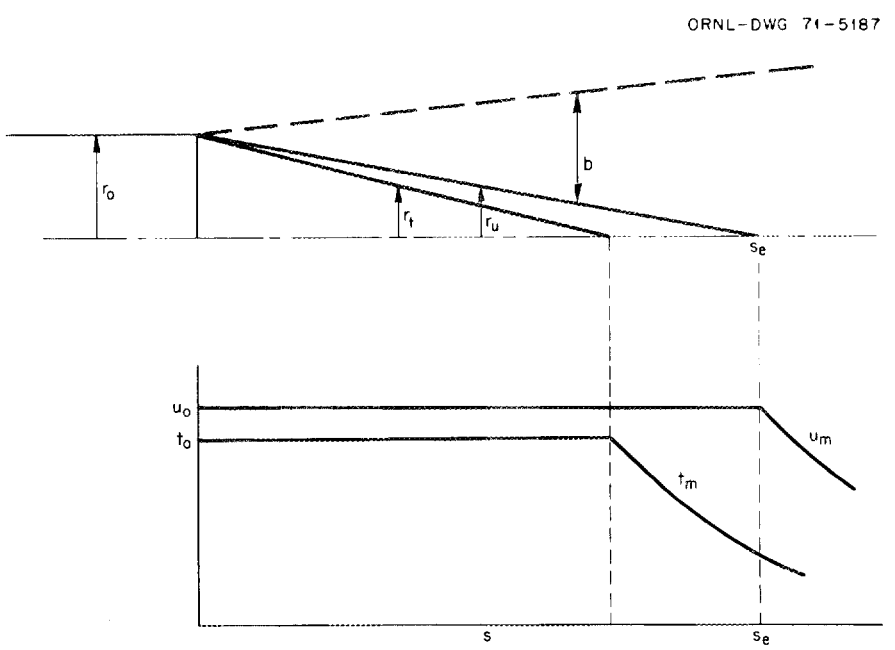

Fig. 6. Zone of Flow Establishment Showing the Potential Cores for Temperature and Velocity.

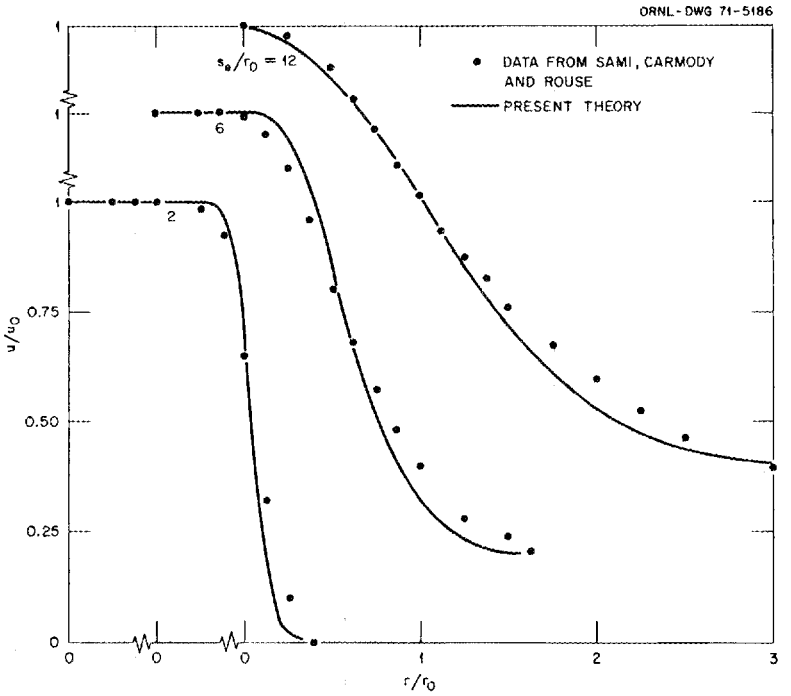

Fig. 7. Velocity Profiles Within the Zone of Flow Establishment for the Simple Momentum Jet. Data are from Sami, Carmody & Rouse (1967).

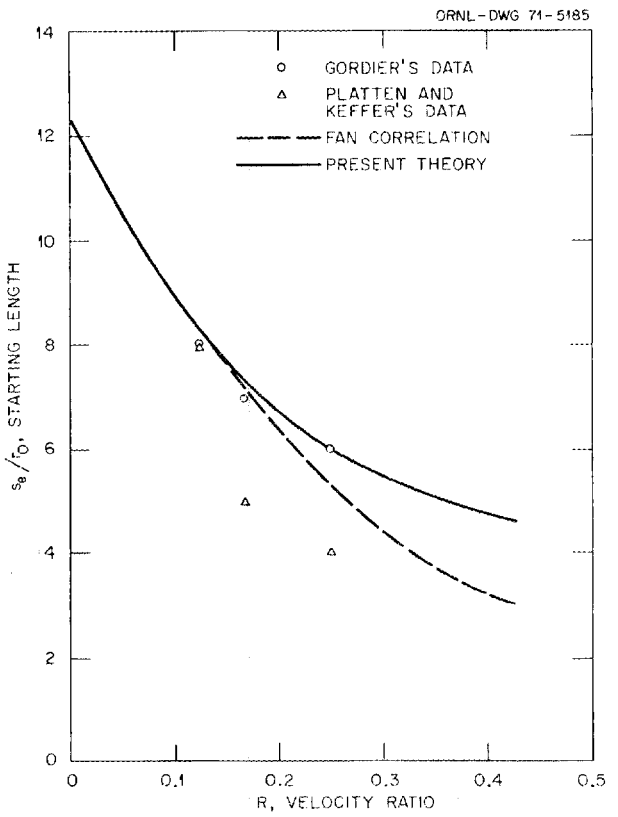

Fig. 8. Starting Length for Non-buoyant Jets Discharged Normal to the Free Stream. Data are from Gordier (1959) and Platten & Keffer (1968).

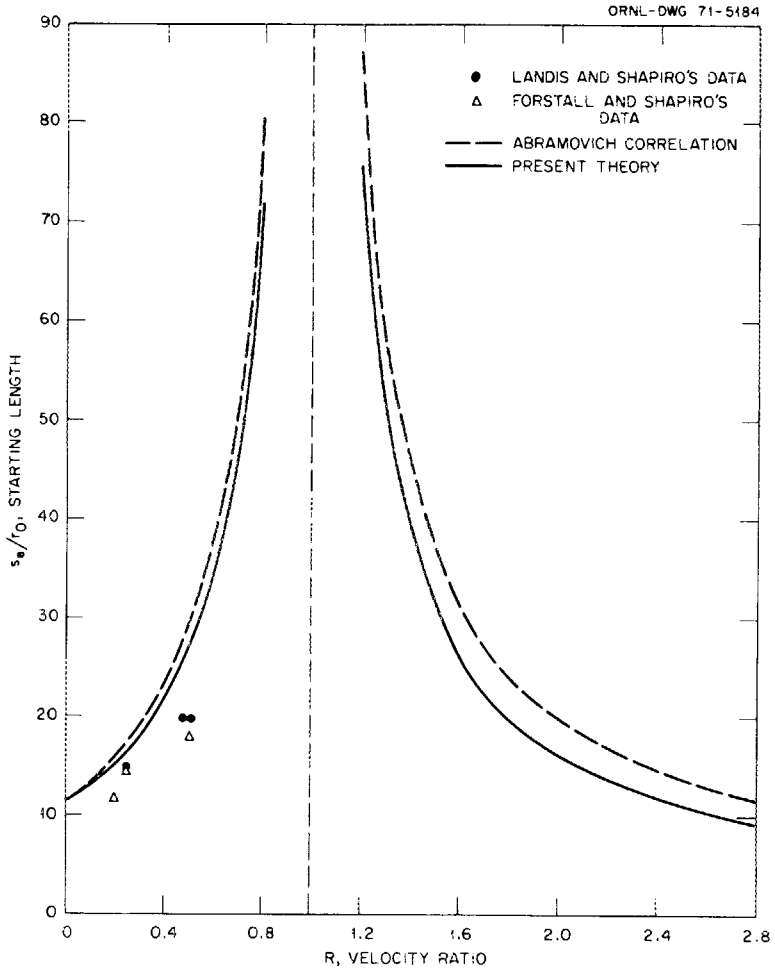

Fig. 9. Starting Length for Non-buoyant Jets Discharged to a Coflowing Stream. Data are from Landis & Shapiro (1951) and Forstall & Shapiro (1950).

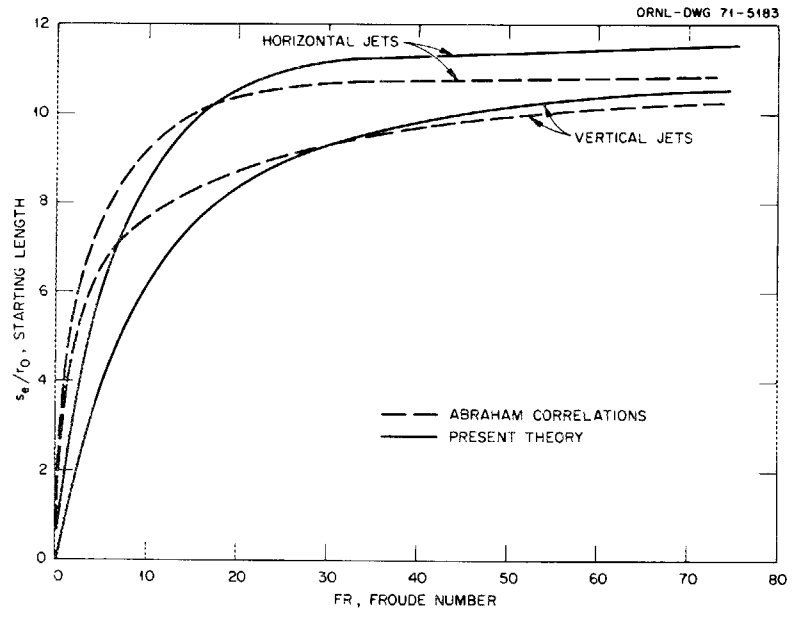

Fig. 10. Starting Length for Buoyant Jets Discharged to a Quiescent Ambient.

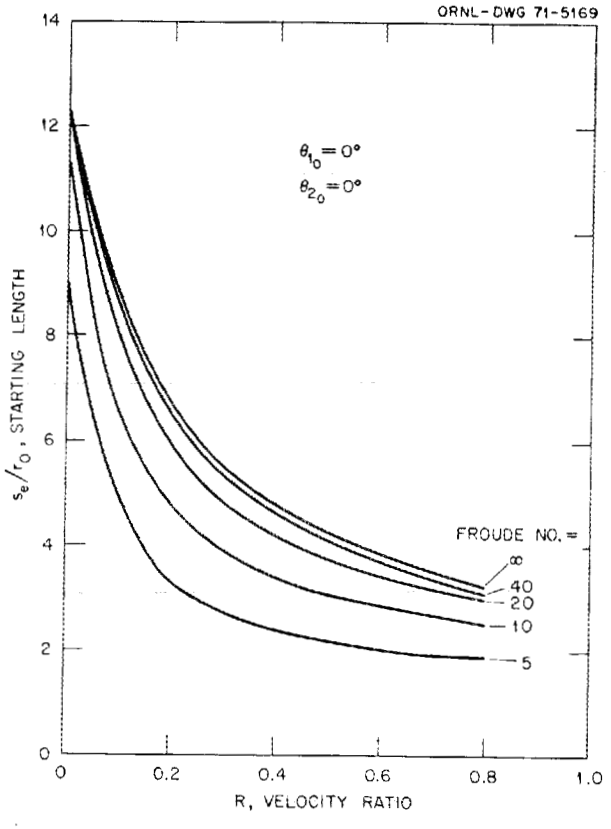

Fig. 11. Starting Length for Horizontal Jets Discharged Normal to the Free Stream.

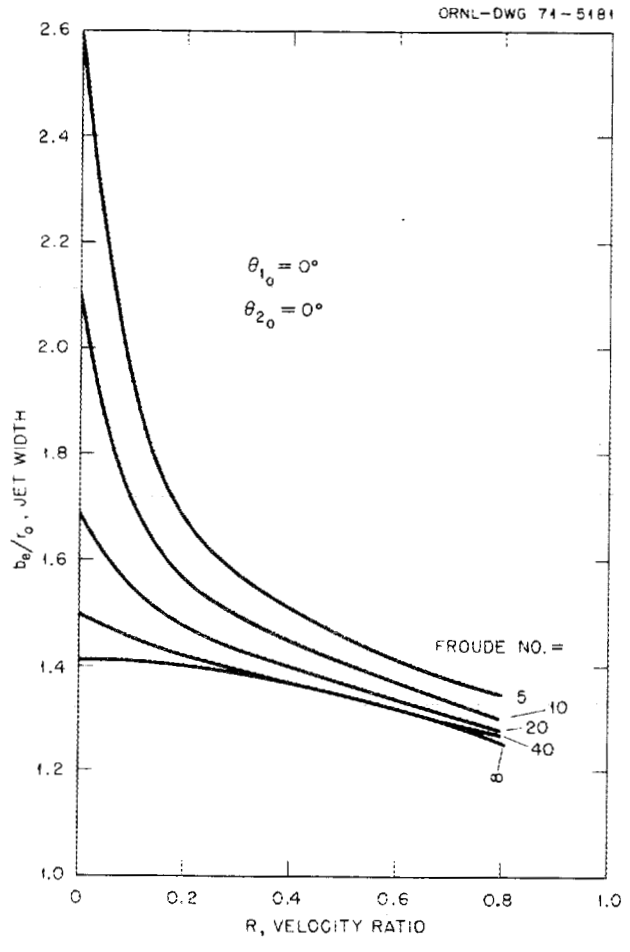

Fig. 12. Jet Width at End of ZFE for Horizontal Jets Discharged Normal to the Free Stream.

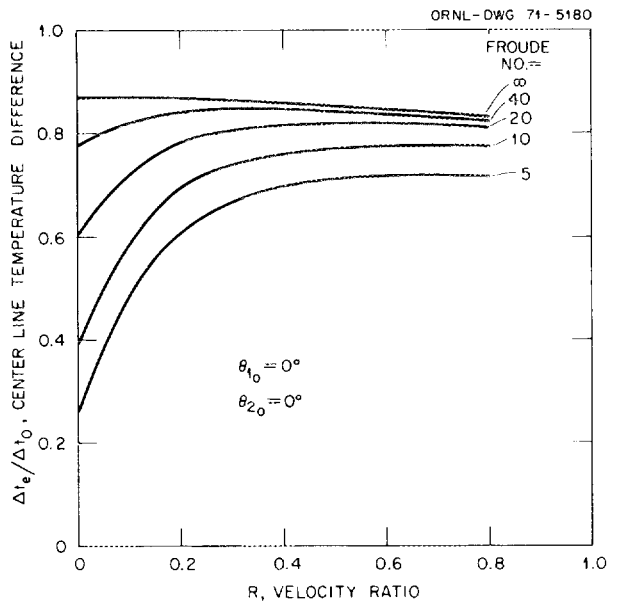

Fig. 13. Centerline Temperature-Difference at End of ZFE for Horizontal Jets Discharged Normal to the Free Stream.

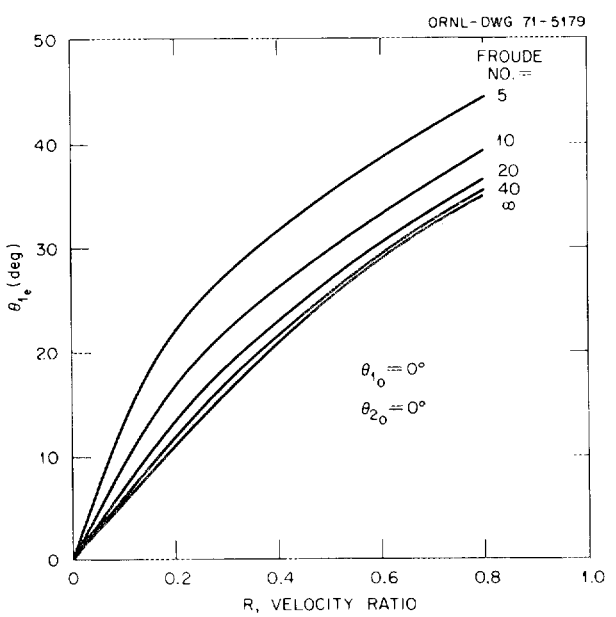

Fig. 14. Θ_1 at End of ZFE for Horizontal Jets Discharged Normal to the Free Stream.

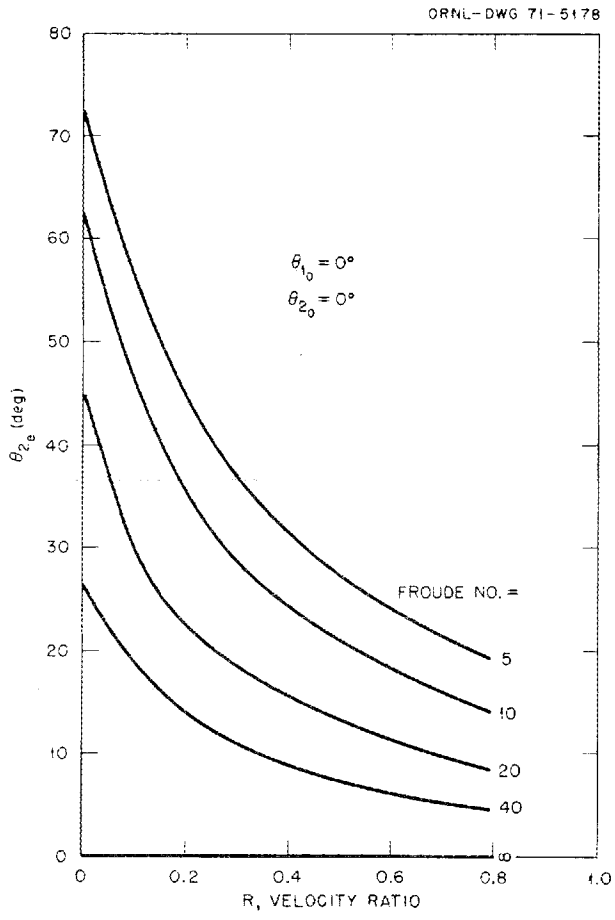

Fig. 15. Θ_2 at End of ZFE for Horizontal Jets Discharged Normal to the Free Stream.

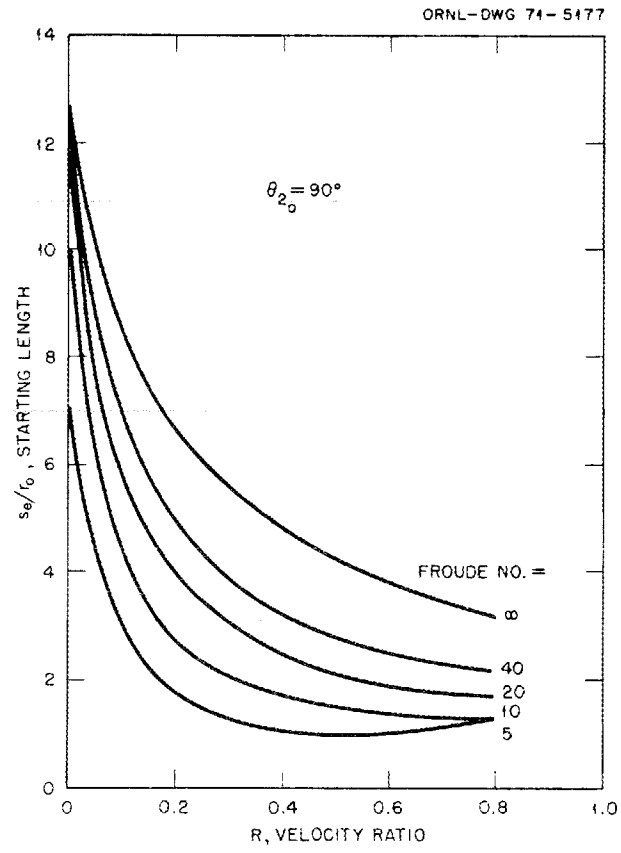

Fig. 16. Starting Length for Vertical Jets Discharged Normal to a Free Stream.

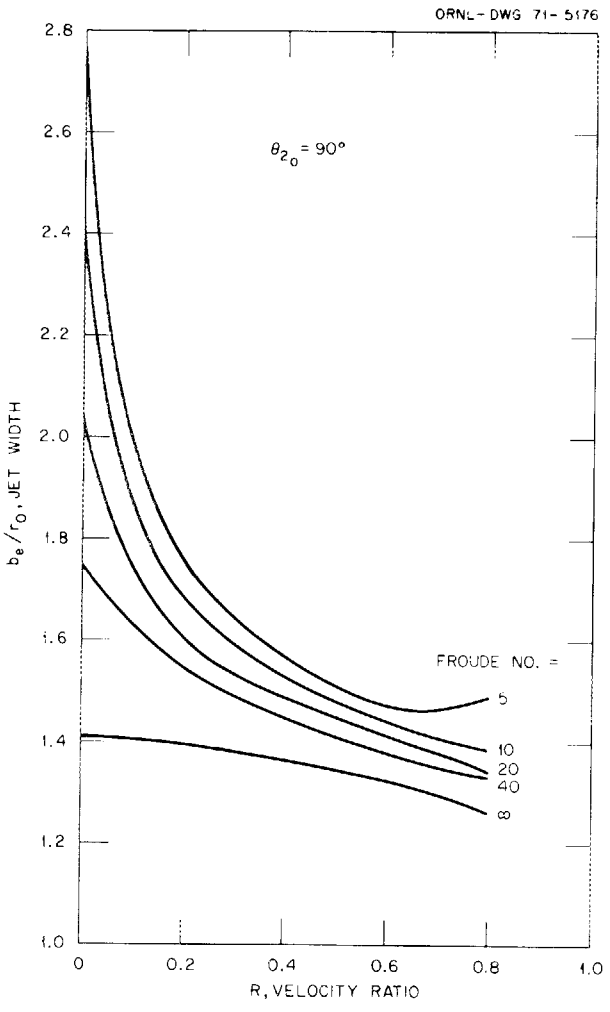

Fig. 17. Jet Width at End of ZFE for Vertical Jets Discharged Normal to a Free Stream.

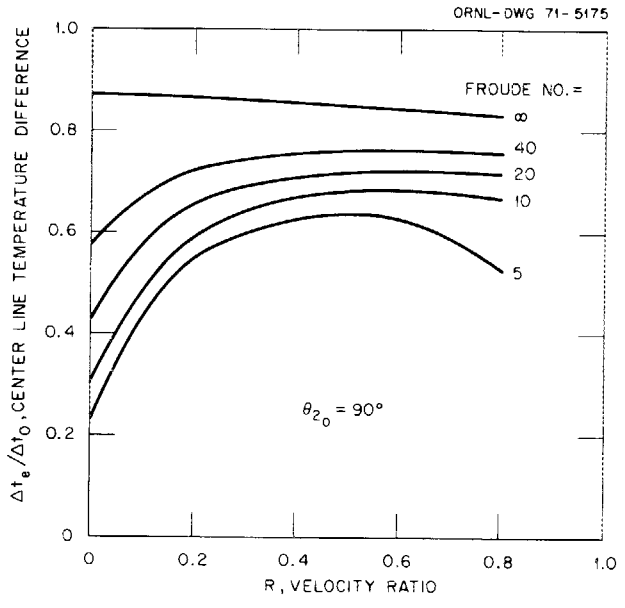

Fig. 18. Centerline Temperature-Difference at End of ZFE for Vertical Jets Discharged Normal to a Free Stream.

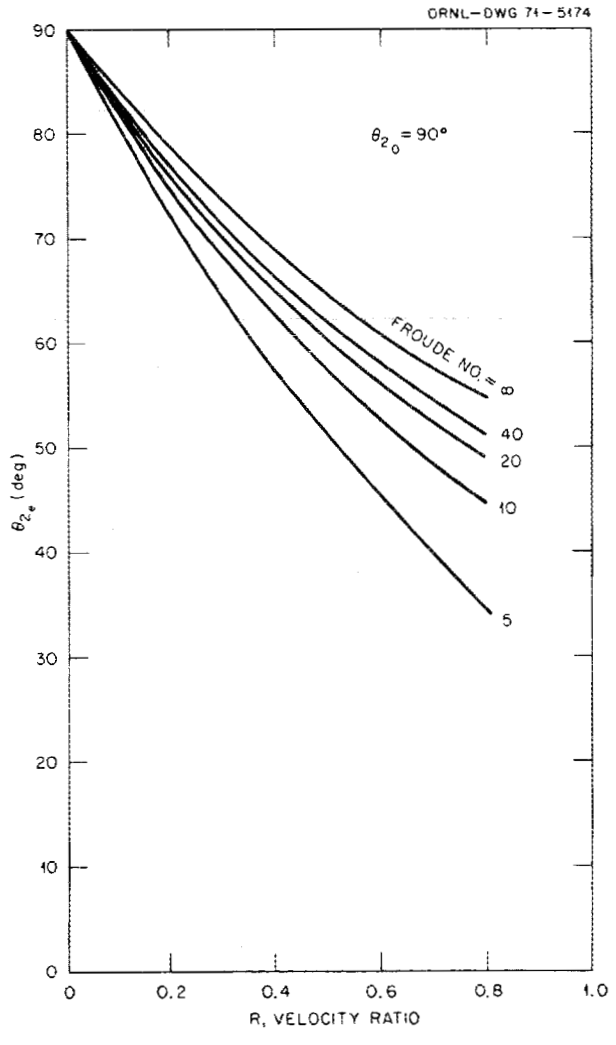

Fig. 19. Θ_2 at End of ZFE for Vertical Jets Discharged Normal to a Free Stream.

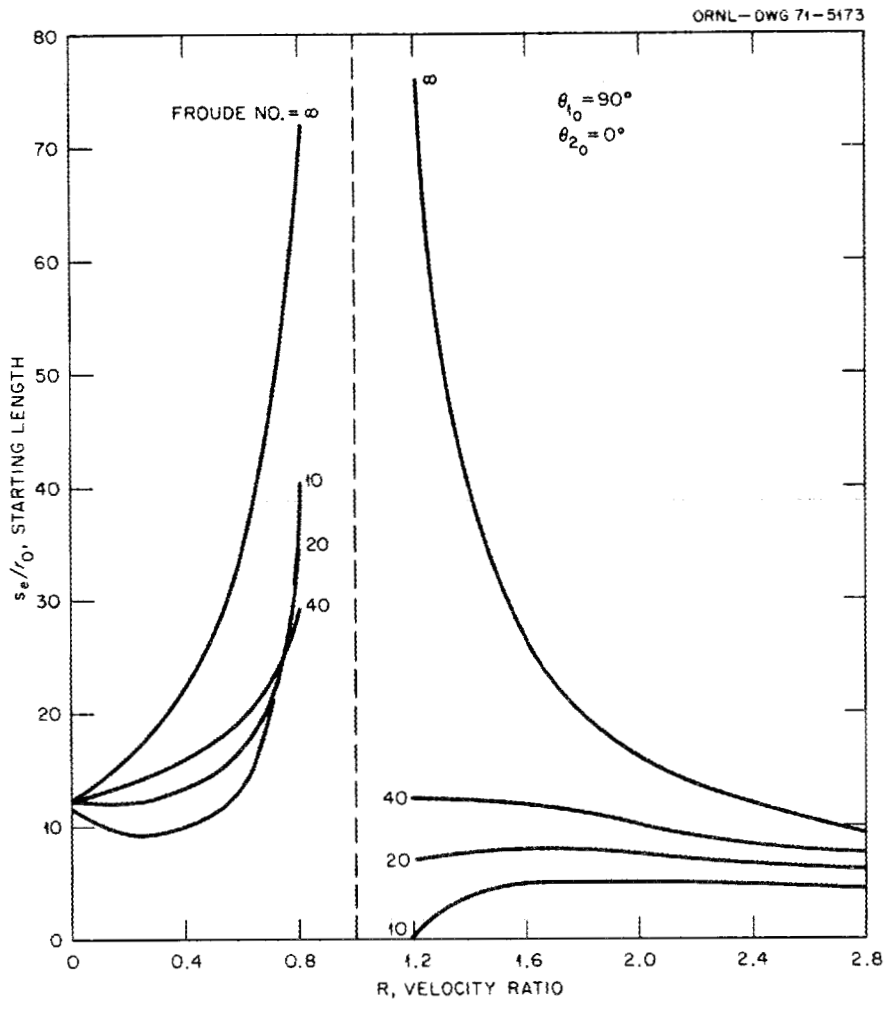

Fig. 20. Starting Length for Horizontal Jets Discharged to a Coflowing Stream.

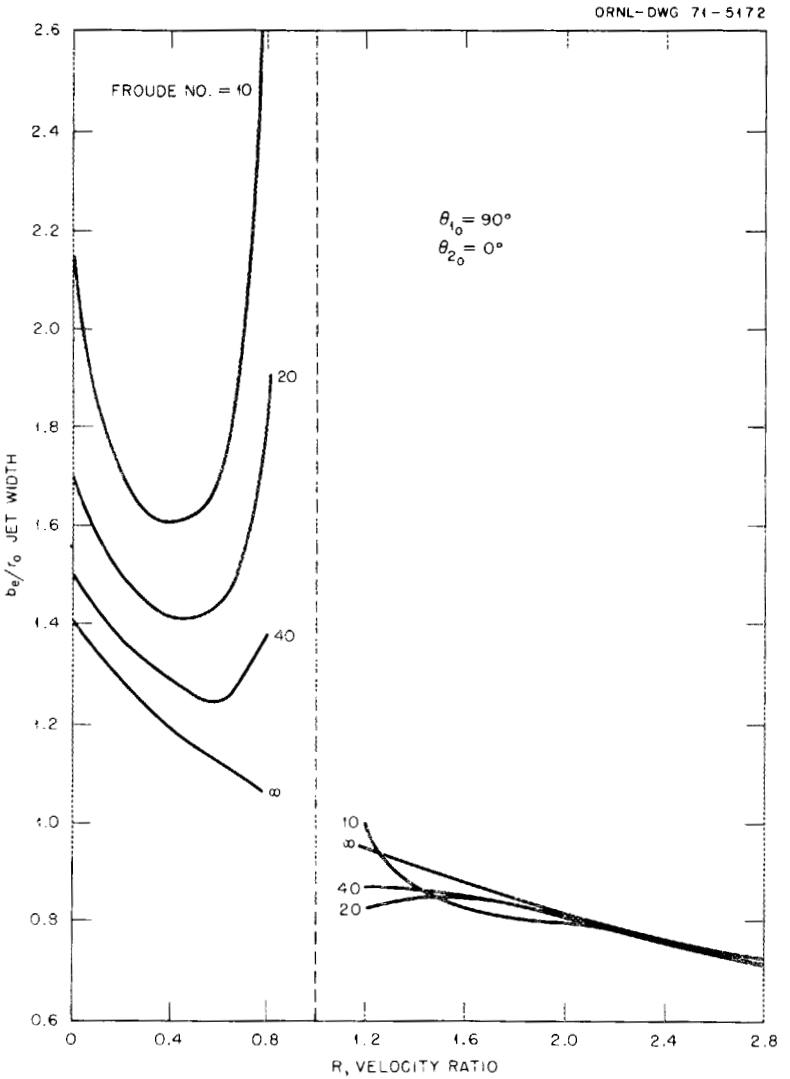

Fig. 21. Jet Width at End of ZFE for Horizontal Jets Discharged to a Coflowing Stream.

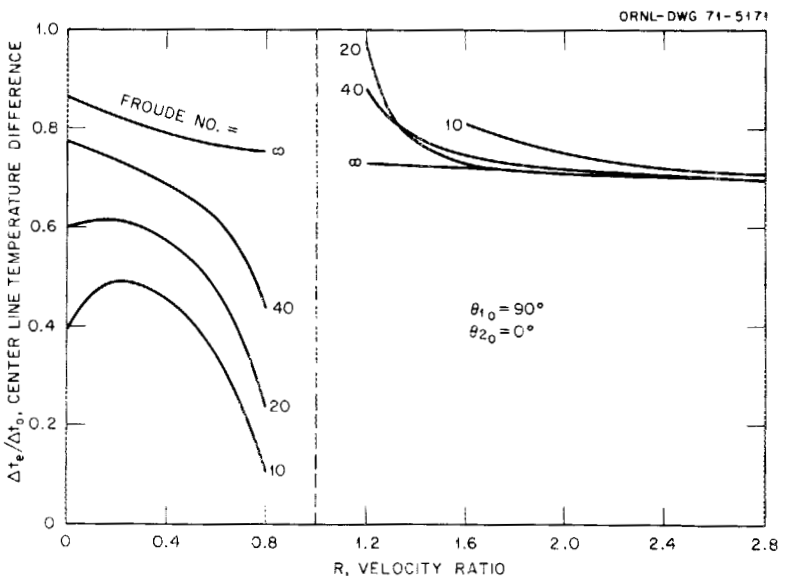

Fig. 22. Centerline Temperature-Difference at End of ZFE for Horizontal Jets Discharged to a Coflowing Stream.

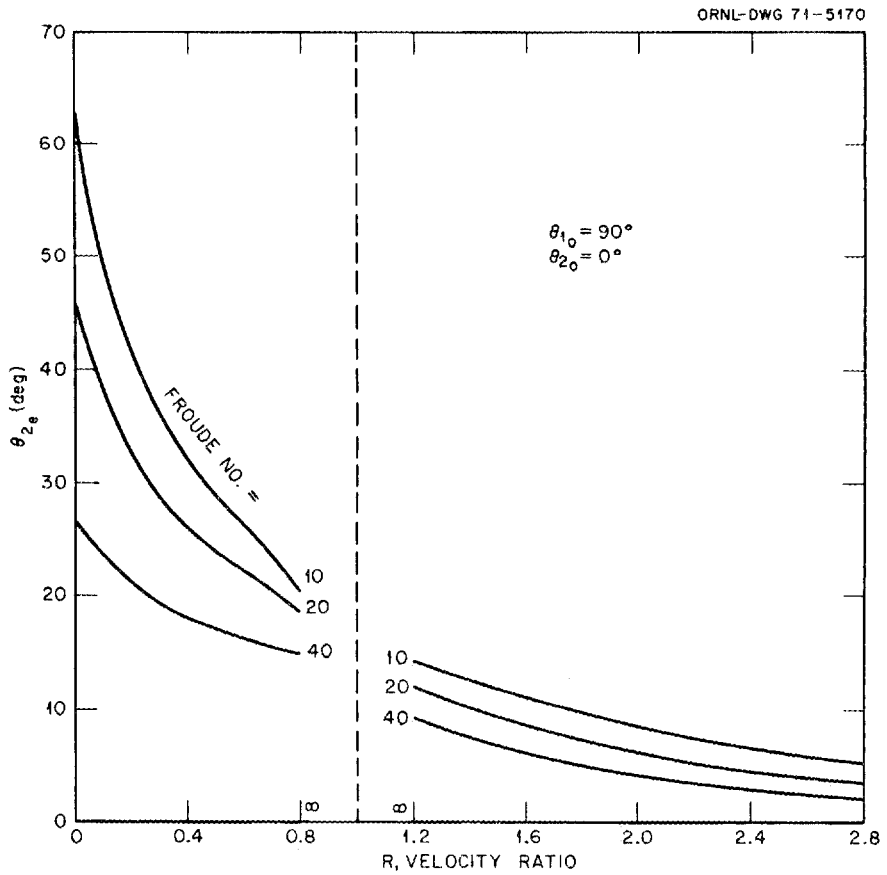

Fig. 23. Θ_2 at End of ZFE for Horizontal Jets Discharged to a Coflowing Stream.

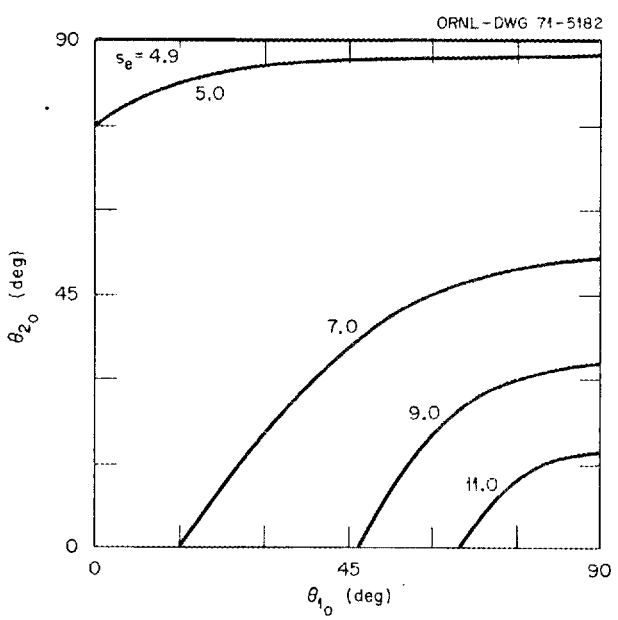

Fig. 24. Starting Length as a Function of Initial Orientation for Buoyant Jets Discharged with Fr = 40, R = 0.2.

INTERNAL DISTRIBUTION

1. S. I. Auerbach
2. S. E. Beall
3. J. R. Buchanan
4. R. S. Carlsmith
5. F. H. Clark
6. C. C. Coutant
7. K. E. Cowser
8. F. L. Culler
9. J. H. Gibbons
10. R. P. Hammond
11–260. E. A. Hirst
261. H. W. Hoffman
262. J. L. Liverman
263. R. N. Lyon
264. B. L. Nichols
265. M. Siman-Tov
266. W. G. Stockdale
267. D. G. Thomas
268. D. B. Trauger
269. G. U. Ulrikson
270. A. M. Weinberg
271. R. P. Wichner
272–296. M. M. Yarosh
297–298. Central Research Library
299. Document Reference Section
300–302. Laboratory Records Department
303. Laboratory Records, ORNL R.C.
304. ORNL Patent Office

EXTERNAL DISTRIBUTION

305. Nathaniel F. Barr, Assistant Director for Radiological Physics, Division of Biology and Medicine, USAEC, Washington, D. C. 20545
306. David F. Cope, RDT-OSR at ORNL
307. Joseph J. DiNunno, Director, Office of Environmental Affairs, USAEC, Washington, D. C. 20545
308. Milton J. Shaw, Director, Division of Reactor Development and Technology, USAEC, Washington, D. C. 20545
309. John R. Totter, Division of Biology and Medicine, USAEC, Washington, D. C. 20545
310. Merrill J. Whitman, Division of Reactor Development and Technology, USAEC, Washington, D. C. 20545
311. William A. Williams, Jr., Division of Reactor Development and Technology, USAEC, Washington, D. C. 20545
312–314. Director, Division of Reactor Licensing
315–316. Director, Division of Reactor Standards
317. Laboratory and University Division, AEC, ORO
318. Patent Office, AEC, ORO
319-320. Division of Technical Information Extension, OR